14

CO_2 Capture and Sequestration

14.1 Introduction

The increasing level of atmospheric carbon dioxide caused by anthropogenic emissions is one of the most pressing problems faced by our planet. About 80% of all CO_2 emissions stem from the combustion of fossil fuels (coal, oil, and natural gas) as evidenced by the steady increase in the burning of fossil fuels and the emission of CO_2 in equal measures over the last century (Figure 14.1) [2]. Further increase in such emissions in the future caused by an increased world population and the economic growth and industrial development of emerging economies is predicted [3]. The resulting need for alternative fuels and the concomitant transition away from carbon-based fossil energy sources has initiated intense research. Realizing the required modifications to the current energy framework can however not be achieved immediately and the large-scale implementation of novel environmentally friendly technologies (e.g. natural gas storage, hydrogen storage, and battery and fuel cell technologies) still requires further development. Thus, there is a demand for efficient CO_2 capture and sequestration (CCS) technologies to lower the CO_2 emission from contemporary energy sources until the energy framework has been adapted to new more environmentally friendly technologies.

The adaptation and implementation of CCS technologies in stationary sources of CO_2 emission such as power plants fired by fossil fuels (e.g. coal and natural gas) appears to be within reach. The generation of electricity from fossil fuels causes about 60% of the worldwide CO_2 emissions [3]. Introducing efficient CCS technologies into the exhaust gas systems of such power plants could therefore lower the worldwide overall CO_2 emissions dramatically. Table 14.1 shows the components of post-combustion flue gas emitted by coal-fired power plants alongside the physical parameters of the emitted gases relevant for carbon capture.

Current technologies for carbon capture from post-combustion flue gas are based mainly on aqueous alkanolamine solutions. A major drawback of this technology with respect to its implementation in power plants is that it carries an energy penalty of approximately 30% of the output of the power plant [4]. This energy loss is associated with the large energy input required to liberate captured CO_2 from the capture medium. As current methods do not allow for

Introduction to Reticular Chemistry: Metal-Organic Frameworks and Covalent Organic Frameworks,
First Edition. Omar M. Yaghi, Markus J. Kalmutzki, and Christian S. Diercks.

Companion website: www.wiley.com/go/yaghi/reticular

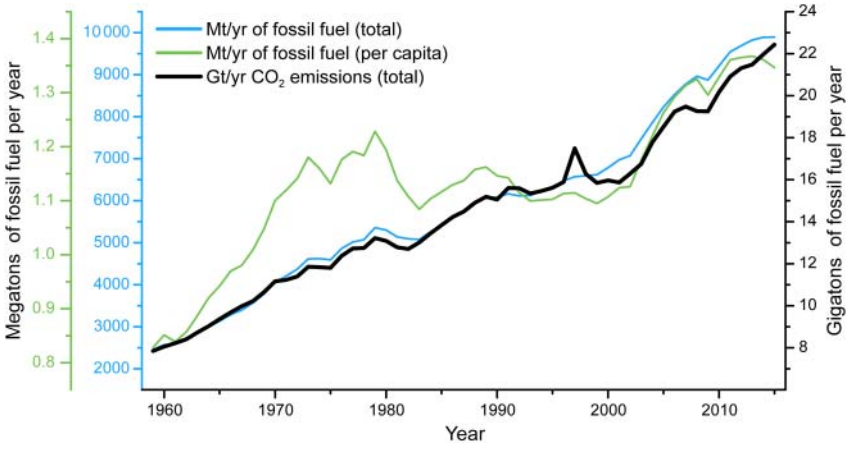

Figure 14.1 Development of the consumption of fossil fuels total (blue line) and per capita (green line) in megatons per year since 1959. The increase in the consumption of fossil fuels correlates with the amount of CO_2 emitted into the atmosphere [1].

Table 14.1 Typical composition of post-combustion flue gas produced by a coal-fired power plant and physical parameters of these gases relevant to the carbon capture process.

Molecule	Flue gas composition (%)	Physical properties			
		Kinetic diameter (Å)	Polarizability (10^{-25} cm^{-3})	Dipole moment (10^{18} esu^{-1} cm^{-1})	Quadrupole moment (10^{26} esu^{-1} cm^{-2})
N_2	73–77%	3.68	17.4	0	1.52
CO_2	15–16%	3.30	29.1	0	4.30
H_2O	5–7%	2.65	14.5	1.85	—
O_2	3–4%	3.46	15.8	0	0.39
SO_2	800 ppm	4.11	37.2–42.8	1.63	—
NO_x [a)]	500 ppm[a)]	—	30.2[a)]	0.316[a)]	—
HCl	100 ppm	3.34	26.3–27.7	1.1086	3.8
CO	20 ppm	3.69	19.5	0.1098	2.5
SO_3	10 ppm	—	—	0	—
Hydrocarbons	10 ppm	—	—	—	—
Hg	1 ppb	—	—	—	—

a) Values for NO_2 and N_2O_4.

the minimization of the input energy required for regeneration of the capture medium it is necessary to develop new materials and methods for CCS with greater energy efficiency [5]. Research in the field of metal-organic frameworks (MOFs) and other reticular framework materials [i.e. zeolitic imidazolate frameworks (ZIFs) and covalent organic frameworks (COFs)] has revealed their

potential toward addressing this challenge. MOFs offer the ability to fine-tune the thermodynamics and kinetics of the CO_2 adsorption/desorption, which is crucial to improving the energy efficiency of CO_2 capture systems. Such modular materials are thus an ideal platform for the development of next-generation CO_2 capture materials [6]. The design principles discussed in earlier chapters provide chemists with the necessary tools to design materials suitable for carbon capture, and further optimize such materials by modifying their structures in pre- and post-synthetic approaches. This structural tunability allows for precise adjustment of the affinity toward CO_2, the optimization of a given material to the composition of post-combustion or pre-combustion flue gas, and even for specific site locations. Since CO_2 capture materials are used in a wide variety of scenarios we will limit this chapter to considerations concerning post-combustion (i.e. CO_2 capture from flue gas) and pre-combustion CO_2 capture (i.e. purification of gases such as syngas). Other fields of application include CO_2 capture from transportation emission and the processing of natural gas (CO_2/CH_4 separation). For further information regarding these applications the reader is referred elsewhere [6, 7]. In this chapter, we will mainly focus on CO_2 capture using MOFs and related materials. In general, similar concepts as those discussed below exist for COFs; however, their performance in this application is limited, arguably due to their nonpolar nature. For more information on CO_2 capture in COFs the reader is referred elsewhere [8].

14.2 *In Situ* Characterization

Knowledge of the specific interactions between the MOF and the gas molecules to be captured is crucial in elucidating means of optimizing MOFs with respect to CO_2 capture. A deep understanding of the relationship between the structural and chemical features of the specific MOF and its adsorption characteristics facilitates the development of next-generation framework materials. Aside from gas sorption experiments, three analytical methods are commonly used to gain insight into the adsorption process and they are described in Section 14.2.1.

14.2.1 X-ray and Neutron Diffraction

The most precise way to acquire structural information with respect to the interaction of gases with the inner surface of a MOF is by using X-ray and neutron diffraction techniques. Both methods allow for the precise determination of the position of gas molecules within the framework. Such data are collected by measuring single crystals or powders of activated MOFs enclosed in a measurement cell (often a capillary) that is evacuated and subsequently filled with a defined quantity of high-purity gas. Diffraction experiments followed by structure solution and refinement allow for the quantification and determination of the precise location of adsorbed gas molecules. This provides information that is essential to the evaluation of the interactions involved in the adsorption process. The structure solution and refinement have the same limitations as those in traditional

diffraction experiments such as the presence of disorder and the adsorption of X-rays (or neutrons) by the measurement cell. In addition to these factors, the stability of the sample upon evacuation and dosing of the adsorbate must be considered. In Sections 14.2.1.1–14.2.1.3 selected examples demonstrating the power of this method are given.

14.2.1.1 Characterization of Breathing MOFs

Certain MOFs show a reversible structural distortion upon CO_2 adsorption where the entire framework structure interchanges between its pristine geometry and an expanded/contracted form in a "breathing" motion. This structural transition is triggered by temperature, pressure, or the interaction of the framework with the dipole or quadrupole moment of an adsorbate (e.g. CO_2 or H_2O) and can be studied by *in situ* powder X-ray diffraction (PXRD). A breathing effect is only possible for certain net topologies (see Chapter 21). Here, we will illustrate the breathing of MIL-53 in the presence of CO_2. MIL-53 is built from rod secondary building units (SBUs) linked by ditopic BDC linkers to form a framework of **sra** topology with trapezoidal channels running along the crystallographic *c*-axis [9]. This structural arrangement allows for expansion and compression of the channels along one direction, which is referred to as breathing of the framework. Figure 14.2 shows an *in situ* PXRD measurement of (Cr)MIL-53 in the presence of CO_2 at different pressures and the corresponding structures. From the powder pattern, one can discern that at CO_2 pressures at or above 4 bar, the pores of the framework open and the structure transitions from the pristine narrow pore (*np*) into a wide pore (*wp*) phase, resulting in a shift of the reflections toward lower angles. This process is reversible;

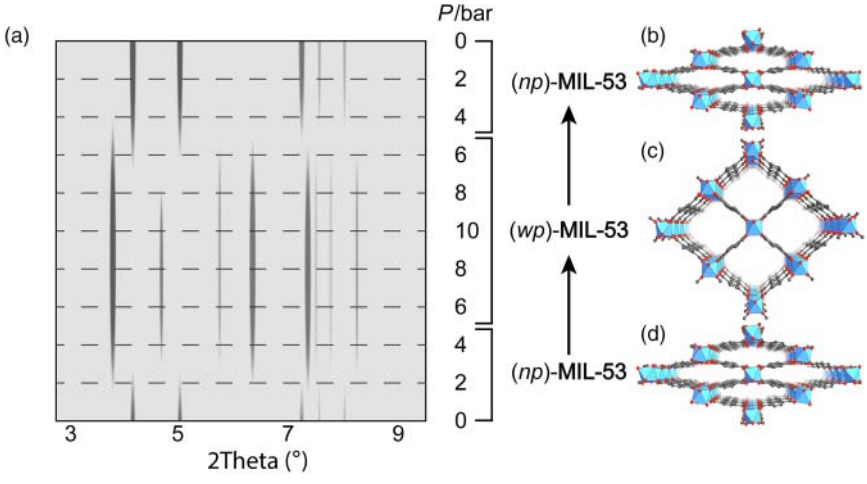

Figure 14.2 Phase transition between the narrow pore (*np*) and wide pore (*wp*) phase of (Cr)MIL-53 upon increasing the CO_2 pressure. (a) The CO_2 pressure-dependent PXRD pattern of (Cr)MIL-53 shows a significant spontaneous shift of the diffraction peaks to lower angles, indicating a phase transition from the *np* to the *wp* phase. (b, d) The *np*-phase is observed up to pressures of 4 bar. (c) At pressures above 4 bar the structure transitions spontaneously into the *wp* phase. All hydrogen atoms are omitted for clarity. Color code: Cr, blue; C, gray; O, red.

after lowering the pressure the framework transitions back to the *np* phase (Figure 14.2). A similar behavior is observed in many other MOFs; however, the synthesis of breathing MOFs in a designed approach has not yet been demonstrated.

14.2.1.2 Characterization of Interactions with Lewis Bases

As mentioned earlier, the central carbon in CO_2 is electrophilic and thus prone to attack by Lewis bases such as amino groups. This interaction can range from weak physisorption to strong covalent interaction (chemisorption) as in the formation of carbamic acid or ammonium carbamate. The former is typically observed for MOFs built from linkers with aromatic amines. An example for such a MOF is $Zn_2(ATZ)_2(OX)$, a framework with a pillared-layered structure comprised of 2D layers of Zn dimers connected by ATZ (5-amino-triazolate) and pillared by OX (oxalate) to form a 3D framework of **pcu** topology (Figure 14.3) [10]. *In situ* single-crystal X-ray diffraction studies of $Zn_2(ATZ)_2(OX)$ in the presence of CO_2 show that the CO_2 molecules interact with the amine moiety in such a way that the CO_2 carbon and the nitrogen of the amine are in close proximity. The C–N distance of about 3.15 Å and the linear molecular geometry of CO_2 indicate that the interaction is best described as physisorption.

14.2.1.3 Characterization of Interactions with Open Metal Sites

The oxygen atoms in CO_2 can interact with Lewis acidic open metal sites. Such open metal sites are found in the structure of (Ni)MOF-74 after the removal of terminal water molecules from its rod SBUs (Figure 14.4; for more detail see Chapter 2). After complete activation, the hexagonal pores of (Ni)MOF-74 are lined with open metal sites. This results in a comparatively high heat of adsorption ($Q_{st} = 42$ kJ mol^{-1}) and a high CO_2 uptake at low pressures (23.9 wt% at 1 bar

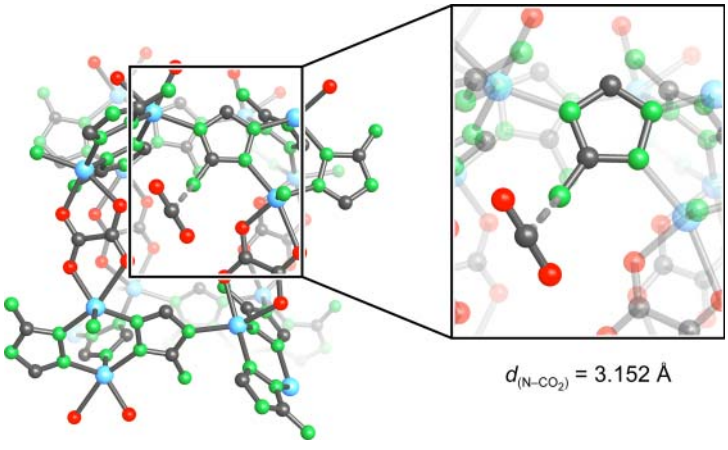

Figure 14.3 Adsorption of CO_2 in $Zn_2(ATZ)_2(OX)_2$. CO_2 is strongly adsorbed on the amines pointing into the pores. The distance between the amine and CO_2 of 3.152 Å indicates strong physisorption. Only one cage and one adsorbed CO_2 molecule are shown. All hydrogen atoms are omitted for clarity. Color code: Zn, blue; C, gray; N, green; O, red.

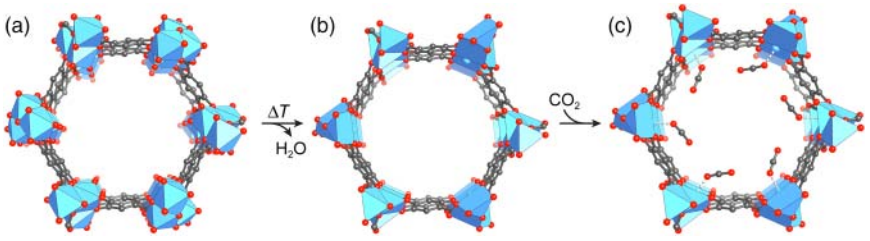

Figure 14.4 (a) Hexagonal pore of (Ni)MOF-74 with view along the crystallographic *c*-axis. (b) Heating (Ni)MOF-74 under dynamic vacuum affords the liberation of water and the creation of open metal sites. (c) Open metal sites are highly polar Lewis acidic structural features that facilitate the physisorption of CO_2 as indicated by short Ni···CO_2 distances (2.29 Å) and a deviation of CO_2 from its linear geometry ($\angle_{(O-C-O)} = 162(3)°$). Only one pore is shown and all hydrogen atoms are omitted for clarity. Color code: Ni, blue; C, gray; O, red.

and 296 K) [11]. High-resolution powder X-ray diffraction (HR-PXRD) shows that CO_2 is preferentially bound to the open metal sites in an end-on manner [11b]. The relatively short distance between the open metal site and the CO_2 oxygen of 2.29(2) Å and an O–C–O angle of 162(3)° are indicative of strong interactions (Figure 14.4).

14.2.2 Infrared Spectroscopy

The vibrational bands observed in infrared spectra are reliable indicators for the strength of the interaction between CO_2 and the framework. The asymmetric stretching ($\nu_3 = 2349\,cm^{-1}$) and bending ($\nu_2 = 667\,cm^{-1}$) modes are infrared active, whereas the symmetric stretching mode ($\nu_1 = 1342\,cm^{-1}$) is infrared inactive (Figure 14.5). The number of possible molecular vibrational modes equals $3n - 6$ ($3n - 5$ for linear molecules) where n is the number of atoms in the molecule. According to this, CO_2 has four different vibrational modes; however, only three are listed above. This is because the bending vibration ν_2 can occur in two different directions and is therefore degenerated. This degeneracy is lifted when CO_2 interacts strongly with the adsorption site and its linear symmetry is disrupted. Along with the characteristic ν_3 shifts as a diagnostic tool, IR spectroscopy serves as a probe that is sensitive to subtle changes of the local interactions between CO_2 and its chemical surroundings.

The asymmetric stretching vibration (ν_3) of CO_2 adsorbed on the open metal sites of (Ni)MOF-74 displays a redshift of about $8\,cm^{-1}$ compared to gaseous CO_2. The origin of this redshift is the interaction of the oxygen lone pairs with empty d-orbitals of the Ni^{2+} centers (backbonding). Additionally, a splitting of the bending vibration ν_2 into two distinct signals with an energy separation of about $8\,cm^{-1}$ is observed, which supports the slightly bent geometry of CO_2 obtained from HR-PXRD data. The existence of a bond between the Ni^{2+} open metal sites and the adsorbed CO_2 molecules is evidenced by an additional absorption band at $2408\,cm^{-1}$. This absorption is ascribed to a $\nu_3 + \nu_{M-O}$ combinatorial vibration ($\nu_{M-O} = 67\,cm^{-1}$). Collection of temperature-dependent IR spectra allows for the calculation of the isosteric heat of adsorption from a van't Hoff plot, and the values calculated using this method ($Q_{st} = -47\,kJ\,mol^{-1}$) are

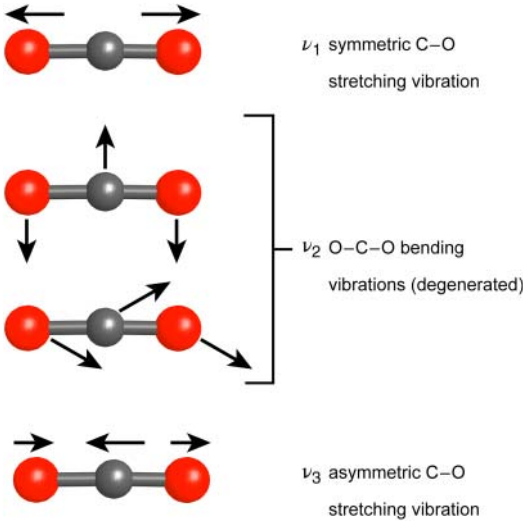

Figure 14.5 (5*n*−3) vibrational modes of CO_2; only three of them are IR active. The bending vibration ν_2 is degenerate in the gas phase and only two IR bands (IR-active vibrational modes) are observed. Strong interactions of CO_2 with an adsorption site can lift the degeneracy of ν_2 due to deviations from the linear molecule geometry, which results in splitting of this adsorption band. Color code: C, gray; O, red.

in good agreement with those calculated from adsorption data for zero coverage ($Q_{st} = -41$ kJ mol^{-1}) [12].

Diffuse reflectance infrared Fourier transform spectroscopy (DRIFTS) is a technique used to analyze the interactions of gas molecules with surfaces and can be employed to study the interactions of CO_2 with amine-functionalized MOFs. We illustrate this with amine functionalized CuBTTri (**the** topology). When fully activated, the structure of CuBTTri has open metal sites that can be functionalized by organic amines such as *N*,*N*′-dimethylethylenediamine (mmen) to give functionalized CuBTTri analogs (mmen-CuBTTri; see Figure 14.6). This functionalized analog exhibits an increased CO_2 uptake compared to pristine CuBTTri due to the chemisorption of CO_2 on the amines in the form of carbamic acid or ammonium carbamate [13].

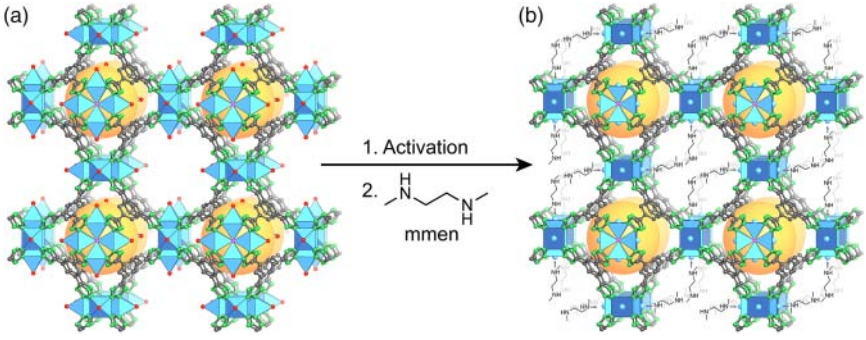

Figure 14.6 (a) Crystal structure of CuBTTri. (b) Activation affords the formation of open metal sites, which can be functionalized using organic diamines such as mmen. The amines dangling into the pores of mmen-CuBTTri can bind CO_2 in the form of carbamic acid resulting in a high selectivity. A drawback of this method is that the amines are only coordinated to the open metals sites and can therefore be exchanged by other potential ligands (e.g. water). The mmen units are drawn as Lewis structures and all hydrogen atoms are omitted for clarity. Color code: Cu, blue; C, gray; N, green; O, red.

Experimentally, the formation of carbamic acid or ammonium carbamate is shown by the disappearance of the N–H stretching vibration at 3282 cm^{-1}. The example of mmen-CuBTTri shows that the modification of framework materials with alkyldiamines can greatly improve the affinity toward CO_2 by strong and selective chemisorption. Interestingly, despite the increased isosteric heat of CO_2 adsorption of mmen-CuBTTri ($Q_{st} = -96$ kJ mol^{-1}) the saturated material is regenerated by temperature swing adsorption (TSA) under mild conditions.

14.2.3 Solid-State NMR Spectroscopy

The previous example (mmen-BTTri) demonstrates that CO_2 can be chemisorbed by amines dangling into the pores of a framework by formation of carbamic acid or ammonium carbamate. Using infrared spectroscopy these two species cannot be distinguished. In contrast, solid-state (cross polarization-magic angle spinning) CP-MAS NMR allows for discrimination between the two, based on a difference in the chemical shift in both the ^{13}C and ^{15}N spectrum. This is typically accomplished by dosing ^{13}C-isotope labeled $^{13}CO_2$ into a MOF synthesized from or modified with ^{15}N-enriched constituents to increase the concentration of NMR-active isotopes. The ^{13}C carbon of carbamic acid has a characteristic NMR shift of $\delta \approx 160$ ppm (which sometimes overlaps with that of the carbamate species at $\delta \approx 164$ ppm). This difference in chemical shift can be used to verify the formation of carbamic acid in IRMOF-74-III(CH_2NHMe) and IRMOF-74-III(CH_2NH_2) upon CO_2 adsorption [14]. Functionalizing the linker in IRMOF-74-III with two primary amines results in an adsorption behavior under dry conditions similar to that of IRMOF-74-III(CH_2NH_2). However, in the presence of water ammonium carbamate is formed (rather than carbamic acid) as indicated by a shift of the carbonyl peak in the ^{13}C MAS NMR spectrum as well as a shift of the amine peak in the ^{15}N MAS NMR spectrum (Figure 14.7) [15].

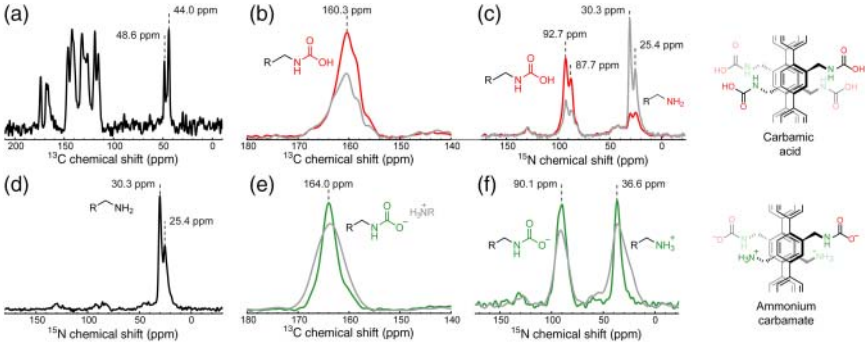

Figure 14.7 (a–c) ^{13}C and (d, c, and f) ^{15}N CP-MAS NMR spectra of isotope-labeled IRMOF-74-III(CH_2NH_2)$_2$ under different measurement conditions (left) and the corresponding chemisorbed species (right). (a, d) Spectra of fully activated IRMOF-74-III(CH_2NH_2)$_2$. (b, c) Spectra after exposure to 675 Torr $^{13}CO_2$ for 24 hours under dry conditions and (e, f) under wet conditions. The gray curves represent the spectra collected after evacuation of the CO_2 treated samples for 24 hours. The corresponding chemisorbed species are shown on the right.

These findings illustrate the power of MAS NMR in distinguishing local chemical surroundings.

14.3 MOFs for Post-combustion CO_2 Capture

In Chapters 2 and 13 we presented an introduction to the general theory of gas adsorption and separation in porous solids. In the following, we will discuss typical structural features that influence the CO_2 capture performance and ways to implement them into MOFs. With respect to CO_2 capture, the design of MOFs and their post-synthetic modification allows the adjustment of the following structural parameters: (i) the presence of open metal sites, (ii) the presence of heteroatoms within the linker and as functionalities appended to the organic backbone or the SBUs, (iii) interactions originating from the SBU, and (iv) the hydrophobicity of the material. For a material to be of interest for CO_2 capture from post-combustion flue gas we must first identify the chemical species present in this type of flue gas (see Table 14.1) to understand the possible interactions they can undergo with the adsorbent. Post-combustion flue gas mainly consists of N_2 (about 77%) and CO_2 (about 16%) and some other minor components such as H_2O, O_2, CO, NO_x, and SO_2. SO_2 is typically removed before the CO_2 capture process. The flue gas is fed to the CO_2 capture material at a pressure of approximately 1 bar and a temperature between 40 and 60 °C. To separate the main components of the gas mixture (i.e. CO_2 and N_2), it is of importance to provide adsorption sites that interact more strongly with CO_2 than with N_2. Since the polarizability (N_2 17.4×10^{-25} cm^{-3}; CO_2 29.1×10^{-25} cm^{-3}) and quadrupole moment (N_2 1.52×10^{26} esu^{-1} cm^{-2}; CO_2 4.30×10^{26} esu^{-1} cm^{-2}) of CO_2 are significantly higher than those of N_2, the separation of these two components following a thermodynamic mechanism is straight forward.

14.3.1 Influence of Open Metal Sites

As illustrated earlier, Lewis acidic open metal sites provide a partial positive charge on the pore surface and are therefore capable of interacting strongly with CO_2. This strong interaction is typically accompanied by high Q_{st} values at low pressures, a high selectivity (in the absence of other molecules with a strong dipole or quadrupole moment), and a high CO_2 uptake. In this context, the most studied group of MOFs with open metal sites is the (M)MOF-74 series (M = Mg^{2+}, Zn^{2+}, Mn^{2+}, Fe^{2+}, and Ni^{2+} among others) [11a, 16]. With 27.5 wt% at 298 K and 1 bar (Mg)MOF-74 has the highest gravimetric uptake of all MOFs in this series [16c]. Every metal center in the rod-like SBUs of MOF-74 (see Chapter 2) has one open metal site and CO_2 binds to these sites in an end-on manner (see Figure 14.4) with an isosteric heat of CO_2 adsorption at zero coverage of −47 kJ mol^{-1}. This is indicative of a strong interaction between the open metal sites and CO_2 and gives rise to the high selectivity for CO_2 in CO_2/N_2 mixtures [12a, 17]. In real world applications, however, flue gas often

contains a low percentage of water (about 7%). Water is a very polarizable molecule with a strong dipole moment and thus, it also binds very strongly to open metal sites (see Table 14.1). Consequently, the CO_2 uptake capacity of (M)MOF-74 materials drops dramatically in the presence of water. To mitigate the water problem other polarizable adsorption sites such as Lewis bases that cannot interact with water must be introduced.

14.3.2 Influence of Heteroatoms

14.3.2.1 Organic Diamines Appended to Open Metal Sites

The coordinative functionalization of Lewis acidic open metal sites by amines is known for many MOFs [13, 18]. One such example was discussed earlier in this chapter where the open metal sites in CuBTTri are functionalized using ethylenediamine (en) or mmen to afford en-CuBTTri and mmen-CuBTTri, respectively (see Figure 14.6). Interestingly, both amine functionalized MOFs exhibit an increased CO_2 uptake capacity and higher Q_{st} values when compared to the parent CUBTTri. Similar results are observed for other MOFs functionalized in this way, but most of them suffer from the gradual loss of the coordinated amines over time. In all these materials CO_2 binds to the appended amine dangling in the pore by formation of carbamic acid or ammonium carbamate.

In contrast, alkylethylenediamine-appended variants of Mg_2(DOBPDC) (DOBPDC = 4,4′-dioxidobiphenyl-3,3′-dicarboxylate) adsorb CO_2 with a unique cooperative adsorption mechanism involving the insertion of CO_2 in the N–metal bond by formation of ammonium carbamate chains [19]. The structure of Mg_2(DOBPDC) is shown in Figure 14.8a, the cooperative adsorption mechanism of CO_2 is depicted in Figure 14.8b. The cooperative adsorption leads to a step-shaped isotherm allowing for high working capacities under TSA conditions. Near complete CO_2 desorption of Mg_2(DOBPDC) is realized by heating to 100 °C. This enables a high CO_2 working capacity of 9.1 wt% with a

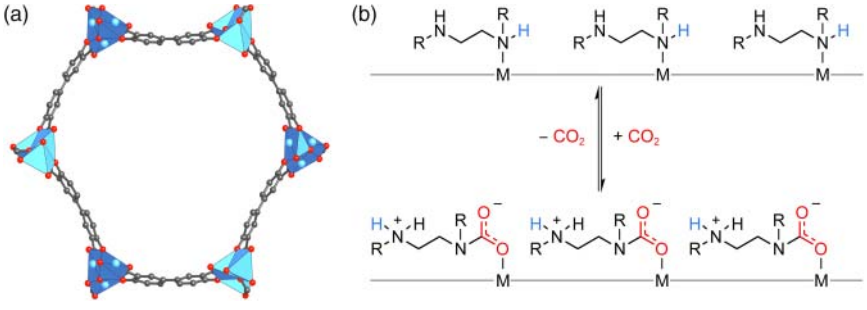

Figure 14.8 Cooperative adsorption mechanism of CO_2 in Mg_2(DOBPDC). (a) The structure of Mg_2(DOBPDC) contains 1D hexagonal channels lined with open metals sites. These open metal sites are functionalized with a series of diaminoalkanes. (b) Schematic adsorption mechanism by insertion of CO_2 into the N–metal bond and formation of ammonium carbamate. Color code: Mg, blue; C, gray; O, red.

modest TSA of only 60 °C. Additionally, the region of steep uptake can be shifted by appending different alkylethylenediamines to the open metal sites.

Even though amine-grafted MOFs show both a higher uptake and high selectivity for CO_2, they generally still suffer from a decrease in adsorption capacity in the presence of water since water can partially replace the diamine grafted onto the open metal site.

14.3.2.2 Covalently Bound Amines

Similar to diamines appended to open metal sites, attaching Lewis basic functional groups with high polarity or even nucleophilic character to the organic backbone of the linker has a stark influence on the CO_2 uptake, as well as on the adsorption mechanisms. An illustrative example for this type of functionalization is amine functionalized (Mg)IRMOF-74-III. (Mg)IRMOF-74-III(CH_2NH_2) has an uptake of 12.5 wt% at 298 K and 1 bar. This might not be as high as the capacity of (Ni)MOF-74; however, in contrast to (Ni)MOF-74, which shows a dramatic decrease of the CO_2 capacity under wet conditions, the performance of (Mg)IRMOF-74-III(CH_2NH_2) is retained [14]. Figure 14.9 shows a breakthrough experiment for (Mg)IRMOF-74-III(CH_2NH_2) that reveals a dynamic adsorption capacity of up to 0.8 mmol g^{-1}, equaling a breakthrough time of 670 ± 10 s g^{-1}.

14.3.3 Interactions Originating from the SBU

The SBUs of MOFs are typically highly polar and strong interactions can arise from these units even in the absence of open metal sites. SIFSIX-2-Cu-i ($Cu(4,4'\text{-dpa})_2(SiF_6)$), a compound built from square $[Cu_2(H_2O)_2](DPA)_{4/2}$ (DPA = 4,4′-dipyridylacetylene) grids that are pillared by SiF_6 units to form a **pcu** net, exhibits the highest CO_2 uptake for any framework material without open metal sites (see Figure 2.12) [20]. The uptake of 19.2 wt% at 298 K and atmospheric pressure is ascribed to interactions of CO_2 with the SiF_6 units. This is supported by the finding that its non-interpenetrated counterpart (SIFSIX-2-Cu) shows a lower CO_2 uptake, and SIFSIX-1-Cu, an isoreticular MOF based on the shorter BIPY (4,4′-bipyridine) linker, shows a comparable CO_2 uptake [21].

Another strategy to increase the interaction between CO_2 and the nonmetallic part of the SBU is to introduce monodentate hydroxyl moieties as capping ligands [22]. An example illustrating the effect of –OH functionalization of the SBUs is the triazolate-based MAF-X25 ($Mn_2{}^{2+}Cl_2$(BBTA), where BBTA = 1*H*,5*H*-benzo(1,2-*d*:4,5-*d*′)bistriazole) shown in Figure 14.10a). MAF-X25 is built from rod SBUs that are connected by BBTA (benzo-bistriazole) linkers to form 1D hexagonal channels. The Co^{2+} centers in the SBUs of MAF-X25 can be oxidized using H_2O_2, which leads to the corresponding –OH functionalized analog MAF-X25-ox ($Mn^{2+}Mn^{3+}(OH)Cl_2$(BBTA); Figure 14.10b). In this example, the introduction of capping hydroxyl groups on the SBU leads to an increase in CO_2 adsorption capacity of up to 50% and a change in the adsorption

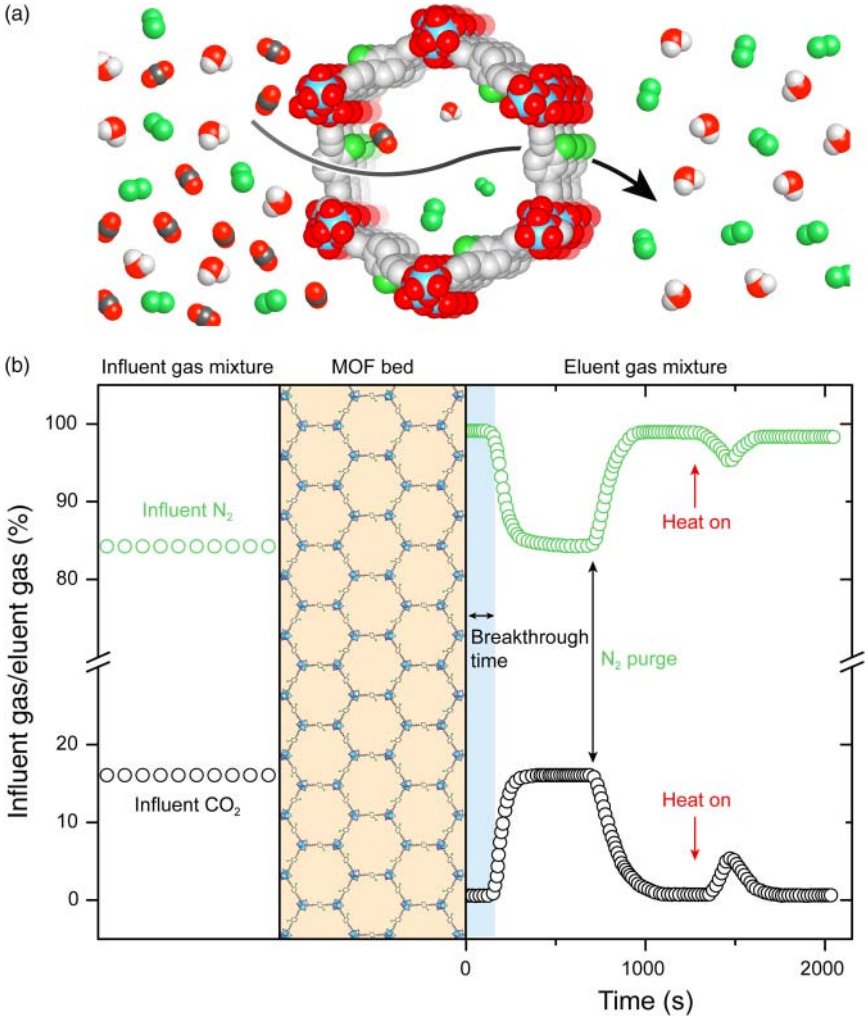

Figure 14.9 (a) Illustration of CO_2 capture by (Mg)IRMOF-74-III(CH_2NH_2). Flue gas is fed to the MOF but only CO_2 is selectively adsorbed. (b) Breakthrough measurement of a N_2/CO_2 (84 : 16) mixture. The MOF adsorbs CO_2 until the working capacity is reached (blue region). Determination of the breakthrough time (s g^{-1}) for a given flow rate allows the calculation of the kinetic gas adsorption capacity (mmol g^{-1}). N_2 purge and subsequent heating regenerate the MOF by liberating all captured CO_2. Color code: Mg, blue; C, gray; O, red.

mechanism. In pristine MAF-X25 CO_2 is adsorbed on the open metal sites while the hydroxyl groups attached to the open metal sites in MAF-X25-ox bind CO_2 covalently as bicarbonate. A similar behavior was observed for the isostructural pair of Mn^{2+} MOFs MAF-X27 and MAF-X27-ox. Interestingly, those materials not only show ultrahigh CO_2 affinity, CO_2 adsorption capacity, and CO_2/N_2 selectivity but also a high cycling stability and good sorption kinetics under dry and wet flue gas conditions.

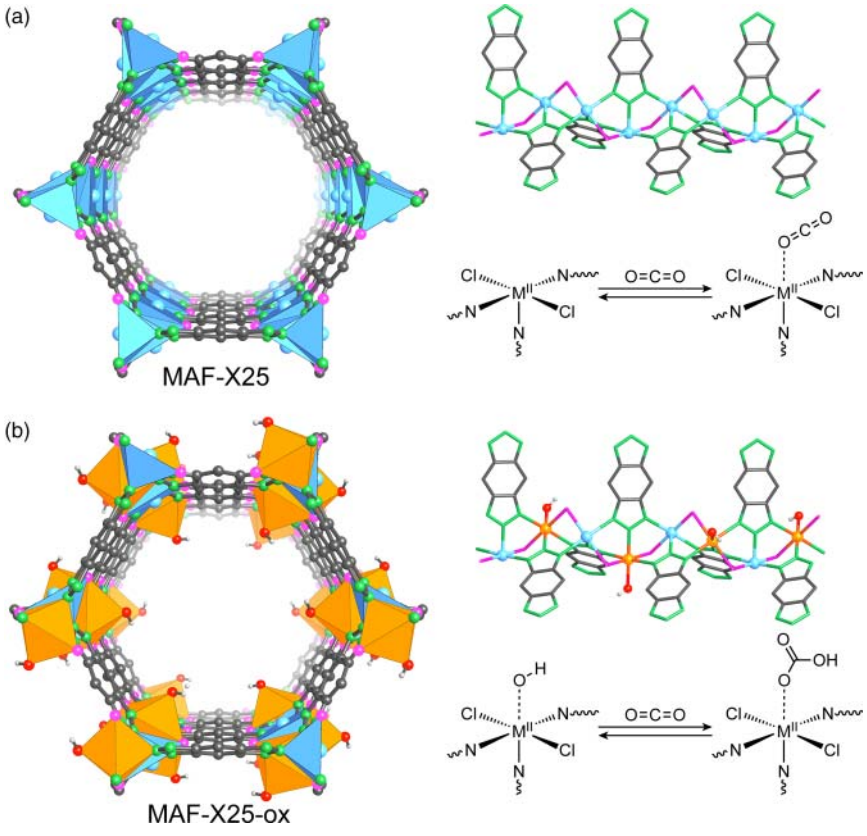

Figure 14.10 Comparison of the adsorption mechanism of CO_2 in MAF-X25 and MAF-X25-ox. (a) In the structure of MAF-X25, CO_2 is adsorbed on the open metal sites generated by activation under dynamic vacuum. (b) The hydroxyl-functionalized open metal sites in MAF-X25-ox bind CO_2 covalently as bicarbonate. Only one pore of the structure is shown and all hydrogen atoms of the linkers are omitted for clarity. Color code: M^{2+}, blue; M^{3+}, orange; C, gray; N, green; O, red; Cl, pink.

14.3.4 Influence of Hydrophobicity

The approaches described above aim at stronger interactions of the framework with CO_2 and therefore higher Q_{st} values to increase the selectivity for CO_2 in the presence of water. Another approach is to prevent water from entering the pores by introducing functionalities that render the pores hydrophobic. To illustrate this approach, we will consider an isoreticular functionalized series of ZIFs: ZIF-300 $Zn(mIM)_{0.86}(bBIM)_{1.14}$ (mIM = 2-methylimidazolate, bBIM = 5-bromo benzoimidazolate), ZIF-301 $Zn(mIM)_{0.94}(cBIM)_{1.06}$ (cBIM = 5-chloro benzoimidazolate), and ZIF-302 $Zn(mIM)_{0.67}(mBIM)_{1.33}$ (mBIM = 5-methyle benzoimidazolate). All three materials are hydrophobic and thus their CO_2 uptake under dry and wet conditions is virtually identical (Figure 14.11) [23]. The drawback of this approach is that materials relying only on hydrophobicity for CO_2/H_2O separation commonly suffer from low CO_2 adsorption capacities due to weak

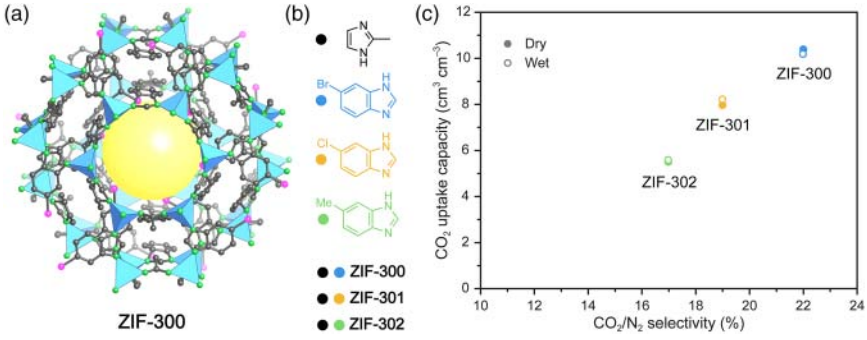

Figure 14.11 (a) Crystal structure of ZIF-300. The molecular structure of the linker molecules and their density in the crystal structure render the resulting materials hydrophobic. (b) Substituted benzimidazolates are used to prepare isostructural ZIFs. (c) Comparison of the CO_2/N_2 selectivity and the CO_2 capacity for ZIF-300, ZIF-301, and ZIF-302 under dry (filled circles) and wet (open circles) conditions. In (a) only one cage is shown and all hydrogen atoms are omitted for clarity. Color code: Zn, blue; C, gray; N, green; Br, pink.

interaction of the framework with CO_2. It would be advantageous to combine all the abovementioned strategies within one material or engineer composites of a hydrophobic shell and a core composed of a material with high selectivity for CO_2 to allow for strong interaction while retaining the initial CO_2 adsorption capacity under wet conditions [24].

14.4 MOFs for Pre-combustion CO_2 Capture

The removal of CO_2 from energy carriers (hydrogen) or fuels (natural gas) is referred to as pre-combustion CO_2 capture. Natural gas, the shifted product of coal gasification, and syngas, produced by steam methane reforming, are both mixtures of various components. The presence of CO_2 in these gas mixtures lowers the energy efficiency when used in combustion processes or fuel cells. Additionally, in the presence of moisture CO_2 is corrosive, which can cause problems with respect to the makeup of containers used. Therefore, it is of interest to purify these gas mixtures by CO_2 separation before the pure gas is either stored or used in power plants, combustion engines, or fuel cells. MOFs suitable for this process, referred to as "sweetening," need to fulfill a set of requirements different from those for post-combustion CO_2 capture. This becomes clear when considering the process conditions and the composition of the gas mixture. Pre-combustion carbon capture is typically carried out at higher pressures (5–40 bar and 40 °C) compared to post-combustion CO_2 capture (about 1 bar) and at a relatively high CO_2 level (e.g. 25–35% for syngas from coal and 15–25% for syngas from methane). This requires MOFs with high CO_2 uptake in the high pressure region [25]. Owing to the larger difference in molecular size in the couples H_2/CO_2 and CH_4/CO_2, kinetic separation (discrimination by pore size)

is applicable to pre-combustion CO_2 capture. However, the small pores needed to achieve high selectivity will cause a significant pressure drop, rendering this approach unattractive for large-scale applications. Therefore, thermodynamic separation is favored, and the general principles of structural optimization are similar to those for carbon capture from post-combustion flue gas outlined in Section 14.3. Since the adsorption takes place at elevated pressures, desorption is often achieved by simply lowering the pressure. Optimization regarding both the selectivity and uptake capacity are needed to render MOFs suitable for industrial applications.

14.5 Regeneration and CO_2 Release

An important part of the CO_2 capture cycle is the release of captured CO_2 from the adsorbent. As discussed earlier in this chapter, the release of captured CO_2 from currently employed capture media (alkanolamine solutions) carries a massive energy penalty rendering those technologies economically unattractive [4]. The ease of regeneration of MOFs, often carried out under comparatively mild conditions, makes them an interesting alternative to solution-based CO_2 capture methods. Common technologies for the regeneration of porous CO_2 capture materials include temperature, vacuum, and pressure swing adsorption (TSA, VSA, and PSA, respectively) or combinations thereof (Figure 14.12). In a typical setup, the CO_2 charged capture material is confined in some sort of cell

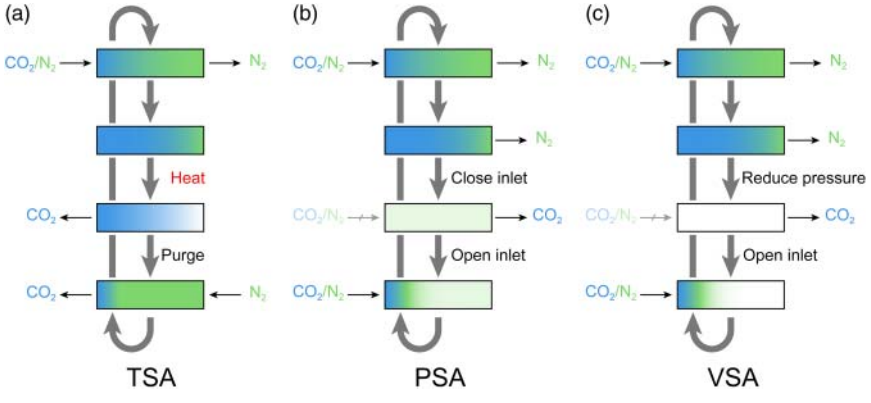

Figure 14.12 Schematic diagrams of temperature swing adsorption (TSA), pressure swing adsorption (PSA), and vacuum swing adsorption (VSA) processes for the regeneration of a fixed bed column used for CO_2 capture from flue gas (N_2/CO_2). (a) The temperature swing adsorption cycle makes use of the different affinities of CO_2 to the adsorbent at different temperatures, facilitating desorption upon increasing the temperature. (b, c) Both pressure and vacuum swing adsorption cycles achieve the regeneration of the adsorbent bed by lowering the partial pressure (closing the inlet valve) or evacuation. This corresponds to moving from the right (high P/P_0) to the left (low P/P_0) on the adsorption isotherm.

or container (e.g. packed bed of powder or pellets) and regenerated by increasing the temperature (TSA) or changing the pressure (PSA and VSA).

14.5.1 Temperature Swing Adsorption

Industrial processes typically produce excess heat that can be used in TSA cycles to regenerate the capture materials that allow for regeneration at low temperatures [26]. By heating the saturated adsorbent at ambient pressure, adsorbed gas molecules desorb from the adsorbent and the increased partial pressure caused by the desorption drives them off the adsorbent bed. An equilibrium state, where no more gas desorbs from the adsorbent, is reached at the optimal desorption temperature of the adsorbent. Desorbed gas molecules remaining in the void spaces of the adsorbent bed are pushed off with a purge, until the desired purity of eluent gas is reached. After cooling the bed to the optimal adsorption/working temperature of the adsorbent the next adsorption cycle is started (Figure 14.12a).

The lower heat capacities of MOFs (about $1\,J\,g^{-1}\,K^{-1}$) compared to conventional monoethanolamine solutions ($3–4\,J\,g^{-1}\,K^{-1}$ depending on the concentration) make them ideal candidates for regeneration by TSA [24, 27]. Regeneration of HKUST-1 by TSA is more successful than regeneration by VSA, which is attributed to the unsuccessful recovery of the open metal sites by VSA [28]. It should, however, be noted that the low thermal conductivity of MOFs may render VSA and PSA more favorable in some cases. This problem is overcome when shaped bodies with appropriate additives, which increase the thermophysical properties of the MOF, are used.

14.5.2 Vacuum and Pressure Swing Adsorption

In PSA and VSA cycles the adsorbent is regenerated by lowering the partial pressure to desorb the captured gas. PSA uses pressures ranging from 8 to 28 bars in the adsorption process whereas the adsorption in VSA is commonly carried out at ambient pressures [25a]. Once the adsorbent is saturated the pressure is lowered. In the case of PSA this is realized by simply closing the inlet valve, which leads to a decrease of the pressure to ambient pressure, whereas in the case of VSA the pressure in the adsorbent bed is lowered to subatmospheric pressures. The adsorbed gas is desorbed by the pressure drop and purged from the adsorbent bed (Figure 14.12b, c). Pressure vacuum swing adsorption (PVSA) can be envisioned as a hybrid of PSA and VSA where an elevated input pressure and a subatmospheric desorption pressure are used. In stationary applications such as power plants post-combustion flue gas is released near ambient pressure, making it necessary to either pressurize the gas for PSA or evacuate the adsorbent bed using VSA. Considering this, TSA represents the most viable process for CO_2 capture from post-combustion flue gas. Pre-combustion carbon capture (e.g. purification of natural gas) typically uses a pressurized gas stream rendering the PSA cycle most appropriate for this application.

Pelletized (Al)MIL-53 that is used in the separation of a mixture of 87% CH_4 and 13% CO_2 at 4 bar and 303 K can be regenerated at 0.1 bar using a PSA cycle yielding methane with 99.4% purity [29]. The regeneration of MOFs by VSA and PVSA is far less studied. In the case of HKUST-1, regeneration using a VSA cycle after exposure to a feed of 13–16% CO_2 in dry N_2 at 2 bar and 308 K is more successful than using a PSA cycle. This is due to the fact that in the VSA cycle all open metal sites are regenerated. The working capacity of HKUST-1 under these conditions is 2.22 mmol g^{-1} with 63% CO_2 recovery [30]. UiO-66 can be regenerated using a PVSA cycle that consists of six consecutive steps: (i) feed pressurization, (ii) adsorption (2 bars and 328 K), (iii) countercurrent blow-down, (iv) concurrent rinse with CO_2, (v) countercurrent evacuation, and (vi) N_2 purge.

14.6 Important MOFs for CO_2 Capture

The performance of an adsorbent with respect to CO_2 capture is characterized by its capacity and selectivity. Since the gas mixtures from which CO_2 is captured contain different gases of similar molecular size, this process is typically based on a thermodynamic separation mechanism and is therefore controlled by the strength of the adsorbate–adsorbent interaction, i.e. the heat of adsorption (Q_{st}). The selectivity and the uptake (in wt%) alongside the primary adsorption sites for MOFs relevant to carbon capture applications are compiled in Tables 14.2 and 14.3, respectively. All values are measured/calculated at low pressure and room temperature conditions similar to those in carbon capture from post-combustion flue gas. From these tables it is clear that MOFs that contain open metal sites or Lewis basic functionalities show higher CO_2 capacities and selectivity. One must keep in mind that open metal sites and diamines appended to them typically lose their selectivity under wet conditions.

The gas uptake determined by adsorption measurements, the Q_{st} values calculation therefrom, and the selectivity calculated using single-component isotherm constitute equilibrium data (see Chapter 13). It is however important to keep in mind that gas separation is a dynamic process and the adsorption/desorption kinetics must be considered in the assessment of a promising adsorbent. For CO_2 capture from flue gas such information is obtained from time-dependent breakthrough experiments. Here, a column filled with activated MOF is exposed to a gas mixture (e.g. CO_2/N_2 simulating flue gas) and the eluent gas breaking through the column is analyzed (see Figure 14.9). Subsequent regeneration of the column can be carried out using any of the abovementioned methods (TSA, PSA, or VSA). Measurements at different concentrations, temperatures, and flow rates provide a more detailed insight into the adsorption/desorption kinetics, information that is useful in the optimization of the parameters relevant for efficient carbon capture (e.g. packing density, structuring of the adsorbent, flow rates, and temperatures, among others).

Table 14.2 Heats of adsorption and selectivity of the best performing MOFs with respect to CO_2 capture.

MOF		CO_2 adsorption selectivity				References
Chemical formula	**Common name**	**Functionality**	**$-Q_{st}$ (kJ mol^{-1})**	**Selectivity**	***T* (K)**	
$H_3[(Cu_4Cl)_3(BTTri)_8(mmen)_{12}]$	mmen- CuBTTri	Amines	96	165	29	[13]
$H_3[(Cu_4Cl)_3(BTTri)_8(en)_{3.75}]$	en-CuBTTri	Amines	90	44	298	[31]
$Cr_3OF(H_2O)_3(BTC)_3$	MIL-101(Cr)	OMS	62	—	—	[32]
$Al(OH)(NH_2\text{-}BDC)$	NH_2-MIL- 53(Al)	Amines	50	—	—	[33]
$Co_2(ade)_2(CO_2CH_3)_2$	bio-MOF-11	Amines	45	65	298	[34]
$Cu_3(TATB)_2$	CuTATB	—	48	24	298	[35]
$Mg_2(DOBDC)$	(Mg)MOF-74	OMS	47	44	303	[12a, 17]
$Ni_2(DOBDC)$	(Ni)MOF-74	OMS	42	30	298	[11, 12b]
$Cu_3(BTC)_2$	HKUST-1	OMS	35	101	293	[36]
Al(OH)(BDC)	MIL-53(Al)	—	35	—	—	[37]
$Cu_3(BTC)_2\cdot 3H_2O$	HKUST-1 (hydrated)	—	30	—	—	[38]
$Zn_4O(NH_2\text{-}BDC)_3$	IRMOF-3	Amine	19	—	—	[39]
$Zn_4O(BDC)_3$	MOF-5	—	17	—	—	[40]
$Zn_4O(BTB)_2$	MOF-177	—	—	4	298	[17]
$Zn_4O(BDC)(BTB)_{4/3}$	UMCM-1	—	12	—	—	[41]

Q_{st} and selectivity for a N_2/CO_2 mixture as well as the primary adsorption sites are given for room temperature and low pressure; conditions similar to those in carbon capture from post-combustion flue gas.

Table 14.3 Gravimetric uptake (wt%) of the best performing MOFs with respect to CO_2 storage.

MOF		CO_2 adsorption capacity				References
Chemical formula	**Common name**	**Primary adsorption site**	**Pressure (bar)**	***T* (K)**	**Uptake (wt%)**	
Mg_2(DOT)	(Mg)MOF-74	OMS	1	298	27.5	[16c]
Zn_2(TDC)$_2$(MA) Zn_2(TDC)$_2$(MA)	Zn_2(tdc)$_2$(MA)	Hybrid	1	298	27.0	[42]
Fe_2(DOT)	(Fe)MOF-74	OMS[a)]	1	298	23.8	[16e]
Mg_2(DOBPDC)	(Mg)IRMOF-74-II	OMS[a)]	1	298	22.0	[19d]
$Al_2(OH)_2$TCPP(Cu)	S_{Cu}	OMS[a)]	1	298	21.7	[43]
(TEPA)$_x$$Mg_2$(DOT)	TEPA-MOF-74	Aliphatic amine	1	298	21.1	[44]
Cu(Me-4py-trz-ia)	Cu(Me-4py-trz-ia)	Hybrid	1	298	21.1	[45]
Cu_3(TDPAT)	Cu-TDPAT	Hybrid	1	298	20.6	[46]
Ni_2(DOT)	(Ni)MOF-74	OMS[a)]	1	298	20.5	[11a]
Cu_3(TDCPAH)	rht-MOF-9	Heteroaromatic amine	1	298	20.2	[47]
Cu_3(BTC)$_2$	HKUST-1	OMS[a)]	1.1	293	19.8	[36a]
Cu[(PYDC$_2$)PdCl$_2$]	NbO-Pd-1	OMS[a)]	1	298	19.7	[48]
Co_2(DOBDC)	(Co)MOF-74	OMS[a)]	1	298	19.7	[11a]
[Mg_2(DOT)(N_2H_4)$_{1.8}$]	N_2H_4-(Mg)MOF-74	Aliphatic amine	1	298	19.5	[49]
Cu_3(TPBTM)	Cu-TPBTM	OMS[a)]	1	298	19.5	[50]
Cu_2(DBIP)	nbo-Cu_2(DBIP)	OMS[a)]	0.95	298	19.3	[51]
[Mg_2(DHT)(H_2O)$_{0.8}$(en)$_{1.2}$]·0.2(en)	CPO-27-Mg-c	Aliphatic amine	1	298	19.2	[52]
Cu(4,4′-dpa)$_2$(SiF_6)	SIFSIX-2-Cu-i	SBU-based interactions	1.1	298	19.2	[20]
Cu_2[(NH_2)-PyrDI]	ZJNU-54	Heteroaromatic amine	1	298	19.1	[53]
Cu(4,4′-bpy)$_2$(SiF_6)	SIFSIX-1-Cu	SBU-based interactions	1	298	19.1	[21]
Cu_6(TADIPA)$_3$	JLU-Liu21	Hybrid	1	298	18.8	[54]
Cu_2(iso-QuDI)	ZJNU-44	Heteroaromatic amine	1	296	18.6	[55]
Cu_2(PDAI)	NJU-Bai21, PCN-124	Hybrid	1	298	18.4	[56]
Zn(BTZ)	Zn(BTZ)	Heteroatom	1	298	18.0	[57]
(PEI)$_x$$Cr_3$(O)OH(BDC)$_3$	PEI-MIL-101	Aliphatic amine	1	298	18.0	[58]

The gravimetric uptake in weight percentage as well as the primary adsorption sites are given for room temperature and low pressure; conditions similar to those in carbon capture from post-combustion flue gas.

a) OMS = open metal site.

14.7 Summary

In this chapter, we discussed different approaches for CO_2 capture from flue gas using MOFs. The different requirements posed to a CCS material by varying compositions of flue gas with respect to the CO_2 capture mechanisms were outlined. We introduced different analytical methods frequently used to characterize the chemical nature of bound CO_2 and thus gain a deeper understanding of possible interactions between CO_2 and MOFs. Using this knowledge, we elucidated the capture mechanisms of MOFs with different structural features, such as open metal sites, –OH functionalized SBUs, and amino functionalities (appended to the SBU or the linker). Different ways for cycled CO_2 adsorption (PSA, TSA, and VSA) were discussed and the chapter concludes with a compilation of MOFs with good CO_2 adsorption properties.

References

1 (a) Le Quéré, C., Andrew, R.M., Canadell, J.G. et al. (2016). Global carbon budget 2016. *Earth System Science Data* 8 (2): 605. (b) Marland, G., Boden, T.A., and Andres, R.J. (2000). Global, Regional, and National Fossil Fuel CO_2 Emissions. Oak Ridge, TN: Carbon Dioxide Information Analysis Center, Oak Ridge National Laboratory, U.S. Department of Energy. (c) Le Quéré, C., Moriarty, R., Andrew, R.M. et al. (2015). Global carbon budget 2014. *Earth System Science Data* 7 (1): 47–85. (d) Houghton, R., Van der Werf, G., DeFries, R. et al. (2012). Chapter G2 Carbon emissions from land use and land-cover change. *Biogeosciences Discussions* 9: 835–878.

2 Edenhofer, O., Pichs-Madruga, R., Sokona, Y. et al. (2015). Intergovernmental panel on climate change. In: *Climate Change 2014: Mitigation of Climate Change*, vol. 3. Cambridge University Press.

3 Pachauri, R.K. and Reisinger, A. (2007). *IPCC Fourth Assessment Report*. Geneva: IPCC.

4 Yu, C.-H., Huang, C.-H., and Tan, C.-S. (2012). A review of CO_2 capture by absorption and adsorption. *Aerosol and Air Quality Research* 12 (5): 745–769.

5 Haszeldine, R.S. (2009). Carbon capture and storage: how green can black be? *Science* 325 (5948): 1647–1652.

6 (a) Li, J.-R., Kuppler, R.J., and Zhou, H.-C. (2009). Selective gas adsorption and separation in metal-organic frameworks. *Chemical Society Reviews* 38 (5): 1477–1504. (b) Morris, R.E. and Wheatley, P.S. (2008). Gas storage in nanoporous materials. *Angewandte Chemie International Edition* 47 (27): 4966–4981.

7 (a) Keskin, S., van Heest, T.M., and Sholl, D.S. (2010). Can metal-organic framework materials play a useful role in large-scale carbon dioxide separations? *ChemSusChem* 3 (8): 879–891. (b) Simmons, J.M., Wu, H., Zhou, W., and Yildirim, T. (2011). Carbon capture in metal-organic frameworks – a comparative study. *Energy & Environmental Science* 4 (6): 2177–2185.

8 Zeng, Y., Zou, R., and Zhao, Y. (2016). Covalent organic frameworks for CO_2 capture. *Advanced Materials* 28 (15): 2855–2873.

9 (a) Millange, F., Serre, C., and Ferey, G. (2002). Synthesis, structure determination and properties of MIL-53as and MIL-53ht: the first Cr^{III} hybrid inorganic–organic microporous solids: $Cr^{III}(OH)\cdot\{O_2C–C_6H_4–CO_2\}\cdot\{HO_2C–C_6H_4–CO_2H\}_x$. *Chemical Communications* 8: 822–823. (b) Serre, C., Millange, F., Thouvenot, C. et al. (2002). Very large breathing effect in the first nanoporous chromium(III)-based solids: MIL-53 or $Cr^{III}(OH)\cdot\{O_2C–C_6H_4–CO_2\}\cdot\{HO_2C–C_6H_4–CO_2H\}_x\cdot H_2O_y$. *Journal of the American Chemical Society* 124 (45): 13519–13526. (c) Serre, C., Bourrelly, S., Vimont, A. et al. (2007). An explanation for the very large breathing effect of a metal-organic framework during CO_2 adsorption. *Advanced Materials* 19 (17): 2246–2251. (d) Boutin, A., Coudert, F.-X., Springuel-Huet, M.-A. et al. (2010). The behavior of flexible MIL-53(Al) upon CH_4 and CO_2 adsorption. *The Journal of Physical Chemistry C* 114 (50): 22237–22244.

10 Vaidhyanathan, R., Iremonger, S.S., Dawson, K.W., and Shimizu, G.K. (2009). An amine-functionalized metal organic framework for preferential CO_2 adsorption at low pressures. *Chemical Communications* 35: 5230–5232.

11 (a) Özgür Yazaydın, A., Snurr, R.Q., Park, T.-H. et al. (2009). Screening of metal-organic frameworks for carbon dioxide capture from flue gas using a combined experimental and modeling approach. *Journal of the American Chemical Society* 131 (51): 18198–18199. (b) Dietzel, P.D., Johnsen, R.E., Fjellvåg, H. et al. (2008). Adsorption properties and structure of CO_2 adsorbed on open coordination sites of metal-organic framework Ni_2(dhtp) from gas adsorption, IR spectroscopy and X-ray diffraction. *Chemical Communications* 41: 5125–5127.

12 (a) Valenzano, L., Civalleri, B., Chavan, S. et al. (2010). Computational and experimental studies on the adsorption of CO, N_2, and CO_2 on Mg-MOF-74. *The Journal of Physical Chemistry C* 114 (25): 11185–11191. (b) Dietzel, P.D., Besikiotis, V., and Blom, R. (2009). Application of metal-organic frameworks with coordinatively unsaturated metal sites in storage and separation of methane and carbon dioxide. *Journal of Materials Chemistry* 19 (39): 7362–7370.

13 McDonald, T.M., D'Alessandro, D.M., Krishna, R., and Long, J.R. (2011). Enhanced carbon dioxide capture upon incorporation of *N*,*N*′-dimethylethylenediamine in the metal-organic framework CuBTTri. *Chemical Science* 2 (10): 2022–2028.

14 Fracaroli, A.M., Furukawa, H., Suzuki, M. et al. (2014). Metal-organic frameworks with precisely designed interior for carbon dioxide capture in the presence of water. *Journal of the American Chemical Society* 136 (25): 8863–8866.

15 Flaig, R.W., Osborn Popp, T.M., Fracaroli, A.M. et al. (2017). The chemistry of CO_2 capture in an amine-functionalized metal-organic framework under dry and humid conditions. *Journal of the American Chemical Society* 139 (35): 12125–12128.

16 (a) Britt, D., Furukawa, H., Wang, B. et al. (2009). Highly efficient separation of carbon dioxide by a metal-organic framework replete with open

metal sites. *Proceedings of the National Academy of Sciences* 106 (49): 20637–20640. (b) Mason, J.A., McDonald, T.M., Bae, T.-H. et al. (2015). Application of a high-throughput analyzer in evaluating solid adsorbents for post-combustion carbon capture via multicomponent adsorption of CO_2, N_2, and H_2O. *Journal of the American Chemical Society* 137 (14): 4787–4803. (c) Bao, Z., Yu, L., Ren, Q. et al. (2011). Adsorption of CO_2 and CH_4 on a magnesium-based metal organic framework. *Journal of Colloid and Interface Science* 353 (2): 549–556. (d) Caskey, S.R., Wong-Foy, A.G., and Matzger, A.J. (2008). Dramatic tuning of carbon dioxide uptake via metal substitution in a coordination polymer with cylindrical pores. *Journal of the American Chemical Society* 130 (33): 10870–10871. (e) Märcz, M., Johnsen, R.E., Dietzel, P.D., and Fjellvåg, H. (2012). The iron member of the CPO-27 coordination polymer series: synthesis, characterization, and intriguing redox properties. *Microporous and Mesoporous Materials* 157: 62–74. (f) Wang, L.J., Deng, H., Furukawa, H. et al. (2014). Synthesis and characterization of metal-organic framework-74 containing 2, 4, 6, 8, and 10 different metals. *Inorganic Chemistry* 53 (12): 5881–5883. (g) Queen, W.L., Hudson, M.R., Bloch, E.D. et al. (2014). Comprehensive study of carbon dioxide adsorption in the metal-organic frameworks M_2(dobdc)(M = Mg, Mn, Fe, Co, Ni, Cu, Zn). *Chemical Science* 5 (12): 4569–4581.

17 Mason, J.A., Sumida, K., Herm, Z.R. et al. (2011). Evaluating metal-organic frameworks for post-combustion carbon dioxide capture via temperature swing adsorption. *Energy & Environmental Science* 4 (8): 3030–3040.

18 (a) Hwang, Y.K., Hong, D.Y., Chang, J.S. et al. (2008). Amine grafting on coordinatively unsaturated metal centers of MOFs: consequences for catalysis and metal encapsulation. *Angewandte Chemie International Edition* 47 (22): 4144–4148. (b) Montoro, C., Garcia, E., Calero, S. et al. (2012). Functionalisation of MOF open metal sites with pendant amines for CO_2 capture. *Journal of Materials Chemistry* 22 (20): 10155–10158.

19 (a) Milner, P.J., Siegelman, R.L., Forse, A.C. et al. (2017). A diaminopropane-appended metal-organic framework enabling efficient CO_2 capture from coal flue gas via a mixed adsorption mechanism. *Journal of the American Chemical Society* 139 (38): 13541–13553. (b) Siegelman, R.L., McDonald, T.M., Gonzalez, M.I. et al. (2017). Controlling cooperative CO_2 adsorption in diamine-appended Mg_2(dobpdc) metal-organic frameworks. *Journal of the American Chemical Society* 139 (30): 10526–10538. (c) McDonald, T.M., Mason, J.A., Kong, X. et al. (2015). Cooperative insertion of CO_2 in diamine-appended metal-organic frameworks. *Nature* 519 (7543): 303–308. (d) McDonald, T.M., Lee, W.R., Mason, J.A. et al. (2012). Capture of carbon dioxide from air and flue gas in the alkylamine-appended metal-organic framework *mmen*-Mg_2(dobpdc). *Journal of the American Chemical Society* 134 (16): 7056–7065. (e) Jo, H., Lee, W.R., Kim, N.W. et al. (2017). Fine-tuning of the carbon dioxide capture capability of diamine-grafted metal-organic framework adsorbents through amine functionalization. *ChemSusChem* 10 (3): 541–550. (f) Lee, W.R., Jo, H., Yang, L.-M. et al. (2015). Exceptional CO_2 working capacity in a heterodiamine-grafted metal-organic framework. *Chemical Science* 6 (7): 3697–3705. (g) Lee, W.R., Hwang, S.Y.,

Ryu, D.W. et al. (2014). Diamine-functionalized metal-organic framework: exceptionally high CO_2 capacities from ambient air and flue gas, ultrafast CO_2 uptake rate, and adsorption mechanism. *Energy & Environmental Science* 7 (2): 744–751.

20 Nugent, P., Belmabkhout, Y., Burd, S.D. et al. (2013). Porous materials with optimal adsorption thermodynamics and kinetics for CO_2 separation. *Nature* 495 (7439): 80–84.

21 Burd, S.D., Ma, S., Perman, J.A. et al. (2012). Highly selective carbon dioxide uptake by $[Cu(bpy\text{-}n)_2(SiF_6)]$(bpy-1 = 4,4′-bipyridine; bpy-2 = 1,2-bis(4-pyridyl)ethene). *Journal of the American Chemical Society* 134 (8): 3663–3666.

22 Liao, P.-Q., Chen, H., Zhou, D.-D. et al. (2015). Monodentate hydroxide as a super strong yet reversible active site for CO_2 capture from high-humidity flue gas. *Energy & Environmental Science* 8 (3): 1011–1016.

23 Nguyen, N.T., Furukawa, H., Gándara, F. et al. (2014). Selective capture of carbon dioxide under humid conditions by hydrophobic chabazite-type zeolitic imidazolate frameworks. *Angewandte Chemie International Edition* 53 (40): 10645–10648.

24 Trickett, C.A., Helal, A., Al-Maythalony, B.A. et al. (2017). The chemistry of metal-organic frameworks for CO_2 capture, regeneration and conversion. *Nature Reviews Materials* 2: 17045.

25 (a) Sircar, S. and Golden, T. (2000). Purification of hydrogen by pressure swing adsorption. *Separation Science and Technology* 35 (5): 667–687. (b) Gupta, R.B. (2008). *Hydrogen Fuel: Production, Transport, and Storage*. CRC Press. (c) Liu, K., Song, C., and Subramani, V. (2009). *Hydrogen and Syngas Production and Purification Technologies*. Wiley.

26 (a) Merel, J., Clausse, M., and Meunier, F. (2008). Experimental investigation on CO_2 post-combustion capture by indirect thermal swing adsorption using 13X and 5A zeolites. *Industrial and Engineering Chemistry Research* 47 (1): 209–215. (b) Berger, A.H. and Bhown, A.S. (2011). Comparing physisorption and chemisorption solid sorbents for use separating CO_2 from flue gas using temperature swing adsorption. *Energy Procedia* 4: 562–567.

27 (a) Kloutse, F.A., Zacharia, R., Cossement, D., and Chahine, R. (2015). Specific heat capacities of MOF-5, Cu-BTC, Fe-BTC, MOF-177 and MIL-53 (Al) over wide temperature ranges: measurements and application of empirical group contribution method. *Microporous and Mesoporous Materials* 217 (Suppl. C): 1–5. (b) Mu, B. and Walton, K.S. (2011). Thermal analysis and heat capacity study of metal-organic frameworks. *Journal of Physical Chemistry C* 115 (46): 22748–22754.

28 Ye, S., Jiang, X., Ruan, L.-W. et al. (2013). Post-combustion CO_2 capture with the HKUST-1 and MIL-101 (Cr) metal-organic frameworks: adsorption, separation and regeneration investigations. *Microporous and Mesoporous Materials* 179: 191–197.

29 (a) Ferreira, A.F., Ribeiro, A.M., Kulaç, S., and Rodrigues, A.E. (2015). Methane purification by adsorptive processes on MIL-53 (Al). *Chemical Engineering Science* 124: 79–95. (b) Serra-Crespo, P., Wezendonk, T.A., Bach-Samario, C. et al. (2015). Preliminary design of a vacuum pressure swing

adsorption process for natural gas upgrading based on amino-functionalized MIL-53. *Chemical Engineering and Technology* 38 (7): 1183–1194.

30 Dasgupta, S., Biswas, N., Gode, N.G. et al. (2012). CO_2 recovery from mixtures with nitrogen in a vacuum swing adsorber using metal organic framework adsorbent: a comparative study. *International Journal of Greenhouse Gas Control* 7: 225–229.

31 Demessence, A., D'Alessandro, D.M., Foo, M.L., and Long, J.R. (2009). Strong CO_2 binding in a water-stable, triazolate-bridged metal-organic framework functionalized with ethylenediamine. *Journal of the American Chemical Society* 131 (25): 8784–8786.

32 Llewellyn, P.L., Bourrelly, S., Serre, C. et al. (2008). High uptakes of CO_2 and CH_4 in mesoporous metal-organic frameworks MIL-100 and MIL-101. *Langmuir* 24 (14): 7245–7250.

33 Arstad, B., Fjellvåg, H., Kongshaug, K.O. et al. (2008). Amine functionalised metal organic frameworks (MOFs) as adsorbents for carbon dioxide. *Adsorption* 14 (6): 755–762.

34 An, J., Geib, S.J., and Rosi, N.L. (2009). High and selective CO_2 uptake in a cobalt adeninate metal-organic framework exhibiting pyrimidine-and amino-decorated pores. *Journal of the American Chemical Society* 132 (1): 38–39.

35 Kim, J., Yang, S.-T., Choi, S.B. et al. (2011). Control of catenation in CuTATB-*n* metal-organic frameworks by sonochemical synthesis and its effect on CO_2 adsorption. *Journal of Materials Chemistry* 21 (9): 3070–3076.

36 (a) Aprea, P., Caputo, D., Gargiulo, N. et al. (2010). Modeling carbon dioxide adsorption on microporous substrates: comparison between Cu-BTC metal-organic framework and 13X zeolitic molecular sieve. *Journal of Chemical and Engineering Data* 55 (9): 3655–3661. (b) Wang, Q.M., Shen, D., Bülow, M. et al. (2002). Metallo-organic molecular sieve for gas separation and purification. *Microporous and Mesoporous Materials* 55 (2): 217–230.

37 Bourrelly, S., Llewellyn, P.L., Serre, C. et al. (2005). Different adsorption behaviors of methane and carbon dioxide in the isotypic nanoporous metal terephthalates MIL-53 and MIL-47. *Journal of the American Chemical Society* 127 (39): 13519–13521.

38 (a) Liang, Z., Marshall, M., and Chaffee, A.L. (2009). Comparison of Cu-BTC and zeolite 13X for adsorbent based CO_2 separation. *Energy Procedia* 1 (1): 1265–1271. (b) Liang, Z., Marshall, M., and Chaffee, A.L. (2009). CO_2 adsorption-based separation by metal organic framework (Cu-BTC) versus zeolite (13X). *Energy and Fuels* 23 (5): 2785–2789.

39 Farrusseng, D., Daniel, C., Gaudillere, C. et al. (2009). Heats of adsorption for seven gases in three metal-organic frameworks: systematic comparison of experiment and simulation. *Langmuir* 25 (13): 7383–7388.

40 Choi, J.-S., Son, W.-J., Kim, J., and Ahn, W.-S. (2008). Metal-organic framework MOF-5 prepared by microwave heating: factors to be considered. *Microporous and Mesoporous Materials* 116 (1): 727–731.

41 Mu, B., Schoenecker, P.M., and Walton, K.S. (2010). Gas adsorption study on mesoporous metal-organic framework UMCM-1. *The Journal of Physical Chemistry C* 114 (14): 6464–6471.

42 Lu, Y., Dong, Y., and Qin, J. (2016). Porous pcu-type Zn(II) framework material with high adsorption selectivity for CO_2 over N_2. *Journal of Molecular Structure* 1107: 66–69.

43 Liu, Y., Yang, Y., Sun, Q. et al. (2013). Chemical adsorption enhanced CO_2 capture and photoreduction over a copper porphyrin based metal organic framework. *ACS Applied Materials & Interfaces* 5 (15): 7654–7658.

44 Cao, Y., Song, F., Zhao, Y., and Zhong, Q. (2013). Capture of carbon dioxide from flue gas on TEPA-grafted metal-organic framework Mg_2(dobdc). *Journal of Environmental Sciences* 25 (10): 2081–2087.

45 Forrest, K.A., Pham, T., McLaughlin, K. et al. (2014). Insights into an intriguing gas sorption mechanism in a polar metal-organic framework with open-metal sites and narrow channels. *Chemical Communications* 50 (55): 7283–7286.

46 Li, B., Zhang, Z., Li, Y. et al. (2012). Enhanced binding affinity, remarkable selectivity, and high capacity of CO_2 by dual functionalization of a rht-type metal-organic framework. *Angewandte Chemie International Edition* 51 (6): 1412–1415.

47 Luebke, R., Weseliński, Ł.J., Belmabkhout, Y. et al. (2014). Microporous heptazine functionalized (3,24)-connected rht-metal-organic framework: synthesis, structure, and gas sorption analysis. *Crystal Growth and Design* 14 (2): 414–418.

48 Spanopoulos, I., Bratsos, I., Tampaxis, C. et al. (2016). Exceptional gravimetric and volumetric CO_2 uptake in a palladated NbO-type MOF utilizing cooperative acidic and basic, metal–CO_2 interactions. *Chemical Communications* 52 (69): 10559–10562.

49 Liao, P.-Q., Chen, X.-W., Liu, S.-Y. et al. (2016). Putting an ultrahigh concentration of amine groups into a metal-organic framework for CO_2 capture at low pressures. *Chemical Science* 7 (10): 6528–6533.

50 Zheng, B., Bai, J., Duan, J. et al. (2010). Enhanced CO_2 binding affinity of a high-uptake rht-type metal-organic framework decorated with acylamide groups. *Journal of the American Chemical Society* 133 (4): 748–751.

51 Liang, Z., Du, J., Sun, L. et al. (2013). Design and synthesis of two porous metal-organic frameworks with nbo and agw topologies showing high CO_2 adsorption capacity. *Inorganic Chemistry* 52 (19): 10720–10722.

52 Bernini, M.C., Blanco, A.G., Villarroel-Rocha, J. et al. (2015). Tuning the target composition of amine-grafted CPO-27-Mg for capture of CO_2 under post-combustion and air filtering conditions: a combined experimental and computational study. *Dalton Transactions* 44 (43): 18970–18982.

53 Jiao, J., Dou, L., Liu, H. et al. (2016). An aminopyrimidine-functionalized cage-based metal-organic framework exhibiting highly selective adsorption of C_2H_2 and CO_2 over CH_4. *Dalton Transactions* 45 (34): 13373–13382.

54 Liu, B., Yao, S., Shi, C. et al. (2016). Significant enhancement of gas uptake capacity and selectivity via the judicious increase of open metal sites and Lewis basic sites within two polyhedron-based metal-organic frameworks. *Chemical Communications* 52 (15): 3223–3226.

55 Song, C., Hu, J., Ling, Y. et al. (2015). The accessibility of nitrogen sites makes a difference in selective CO_2 adsorption of a family of isostructural metal-organic frameworks. *Journal of Materials Chemistry A* 3 (38): 19417–19426.

56 Lu, Z., Bai, J., Hang, C. et al. (2016). The utilization of amide groups to expand and functionalize metal-organic frameworks simultaneously. *Chemistry A European Journal* 22 (18): 6277–6285.

57 Cui, P., Ma, Y.-G., Li, H.-H. et al. (2012). Multipoint interactions enhanced CO_2 uptake: a zeolite-like zinc-tetrazole framework with 24-nuclear zinc cages. *Journal of the American Chemical Society* 134 (46): 18892–18895.

58 Lin, Y., Yan, Q., Kong, C., and Chen, L. (2013). Polyethyleneimine incorporated metal-organic frameworks adsorbent for highly selective CO_2 capture. *Scientific Reports* 3: 1859.